Control of Tool/Workpiece Contact Force with Application to Robotic Deburring

THOMAS M. STEPIEN, MEMBER, IEEE, LARRY M. SWEET, MEMBER, IEEE, MALCOLM C. GOOD, AND MASAYOSHI TOMIZUKA, MEMBER, IEEE

Abstract—**The design and implementation of a microprocessor-based system to control the interaction forces between a five-axis articulated robot and a workpiece is described. The control system worked in parallel with a robot controller by calculating position corrections that allowed forces to be controlled in the desired manner. These corrections were successfully interfaced to the controller's position control loop on an individual-axis level. Stable force-control algorithms were designed in spite of limitations imposed by flexibility in the robot drive train. For multi-degree-of-freedom force control, it is shown that each axis can be considered autonomous, obviating the need for a multivariable approach. Force control was implemented in both edge following and deburring experiments. In edge following, the commanded normal force ranged from 1 to 15 N, while the root mean square (rms) force errors remained constant. Errors increased from 0.5 to 1.5 N rms as tangential speed was increased from 1 to 9 cm s^{-1}. The performance of the force control system during deburring operations was characterized across the full force and speed range of the cutting tools used. The smoothness of cut was shown to be consistent with manual deburring operations in terms of optimal feed and metal removal rates.**

I. Introduction

MOST commercially available robots function solely as position control devices with no means of directly controlling the contact forces[1] between the robot's end effector and workpiece. In a number of important manufacturing applications, in particular deburring and assembly, control of the interaction forces is critical. Robotic systems for automated assembly have been discussed extensively in the literature. The emphasis here has fallen on specialized solutions such as use of remote center compliance devices for part insertion. The force control system presented in this paper has applications in a wide range of manufacturing problems because of the system's ability to regulate contact force in an arbitrary orientation relative to a tool mounted on the endpoint of the robot.

Manuscript received November 15, 1984; revised September 27, 1986. An earlier version of this paper was presented at the 1985 IEEE International Conference on Robotics and Automation, St. Louis, MO, USA.

T. M. Stepien was with General Electric Corporate Research & Development, Schenectady, NY, USA. He is now with The Charles Stark Draper Laboratory, Inc., Cambridge, MA, 02139, USA.

L. M. Sweet is with General Electric Corporate Research & Development, Schenectady, NY, 12308, USA.

M. C. Good was a Visiting Research Scientist at General Electric Corporate Research & Development, Schenectady, NY, USA. He is now with the Australian Commonwealth Scientific and Industrial Research Organization, Melbourne, Australia.

M. Tomizuka is with the University of California, Berkeley, CA, 94720, USA.

IEEE Log Number 8611967.

[1] In this paper "force" implies "force and torque."

The particular focus of this paper is the application of force control to robotic deburring of machined and cast parts. Most machining and casting processes leave a raised edge, or burr, that must be removed in finishing operations using rotary files, abrasive grinders, wire brushes, or similar tools. Finishing operations in general are extremely labor intensive; they present excellent opportunities for robotic automation.

Deburring presents three problems preventing the practical use of conventional fixed-path playback robots. The first problem results from progressive wear of the abrasive tool. As the tool wears, the robot will be unable to maintain constant force against a workpiece; after extreme wear the tool may lose contact completely. A second difficulty is the unpredictability of burr size and location. A force control system must be able to remove varying amounts of material as a tool traverses the edge of the workpiece. The third problem involves the complexity of parts, which are often produced by casting operations and numerically controlled machines. Since programming of robot motions for complex parts can be very tedious, force control systems capable of edge following with minimal path teaching are desirable.

In this context the system shown in Fig. 1 was developed for research on robot force control. A General Electric P50 five-axis robot and controller formed the basis of the system. A six-axis force sensor mounted on the endpoint of the robot measured forces, which were inputs to a force control computer. The force controller calculated the position changes necessary to control the forces in the desired manner. These changes were output from the force controller and summed with nominal position commands calculated by the robot controller.

One of the principal design objectives of this force control system was to integrate a supplemental force control architecture with existing robot motion controls. This structure preserved existing programming utilities with which a user specifies the desired nominal path for the end effector. This design approach differs greatly from a structure capable of controlling force without controlling position.

A block diagram of the position control loop of a single robot axis is shown in Fig. 2 [6]. The blocks are as follows

Motion processor contains algorithms which perform path interpolation and coordinate transformation functions. The commanded position output Θ_c is updated every t_0.

Axis processor closes the motor position control loop with

0882-4967/87/0200-0007$01.00©1987 IEEE

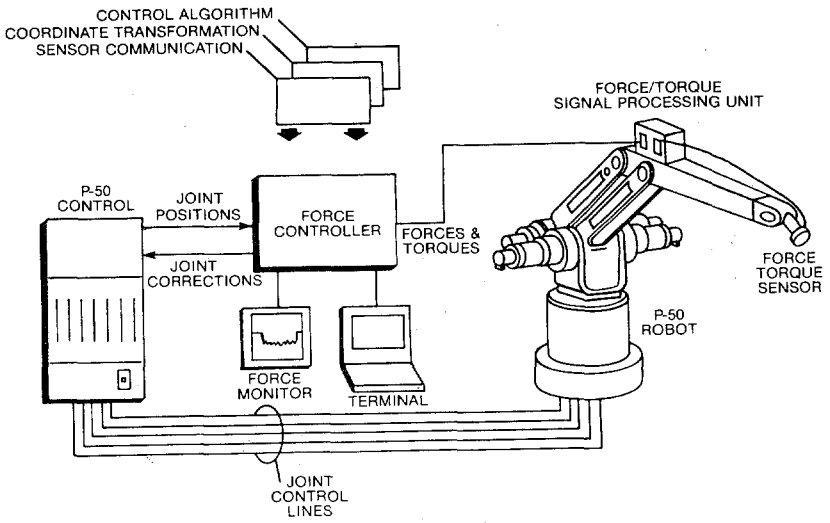

Fig. 1. Schematic of force control system.

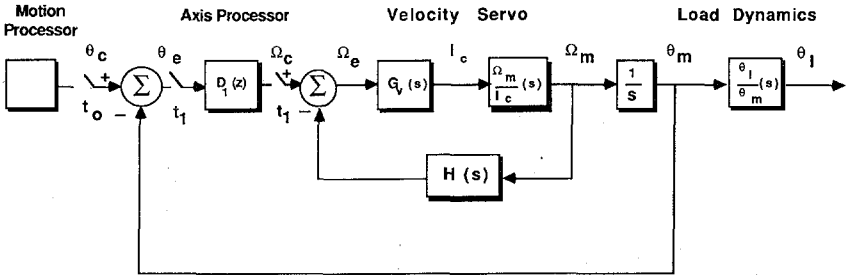

Fig. 2. Block diagram of position control loop.

a sample interval of t_1, interpolating between t_0 intervals. The position error Θ_e, the difference between the commanded position Θ_c and the motor position Θ_m, is the input to the block. The commanded velocity Ω_c is the output.

Velocity servo contains a P*I* velocity controller $G_v(s)$, and the transfer function relating the current command I_c to motor velocity Ω_m. $G_v(s)$ seeks to minimize the velocity error Ω_e, the difference between the commanded velocity Ω_c and motor velocity Ω_m. $H(s)$ represents the dynamics of the tachometer feedback loop.

Load dynamics represents the transfer function between motor position Θ_m and load position Θ_l.

Notice that position control is open loop: there is no feedback of the load position Θ_l to the commanded position Θ_c.

Force control was implemented within this position control structure. The axis processor and velocity servo were left intact to maintain the programming and safety features of the system. Most force control strategies to date presume the feedback and control structure must be multivariable in nature. In this paper we demonstrate the feasibility of force control in a multi-axis, articulated robot using coordinate transformations with force control loops closed *one axis at a time*. This approach yielded feedback control algorithms that were much easier to implement than the general multivariable case and permitted careful tuning of individual axis loops to avoid instabilities induced by drive system resonances.

II. Previous Research

An excellent review of robot force control is presented in [21]. The following are specific comparisons with the present work.

A. Hybrid Position/Force Control

Hybrid position/force control partitions the force control problem using a set of position and force constraints depending on the mechanical and geometric characteristics of the performed task [12]. Position constraints exist along the normal to a surface where the presence of a surface constrains the range of motion. Force constraints exist along surface tangents where it is impossible to apply arbitrary levels of force. The motion of an end effector in contact with the surface is thus partitioned by orthogonal sets of constraints. Motion control satisfying these constraints simultaneously is the basis of this technique.

Raibert and Craig [4], [16] describe hybrid control with the position and force loops operating under different control laws (PID for position and PI for force) to control a manipulator. Position was measured with joint-mounted sensors (encoders) and force with a wrist-mounted strain gauge sensor. Position and force errors were multiplied by a compliance selection matrix, which informed the controller whether degrees-of-freedom of the task were position or force constrained. Control was implemented on two axes of a Scheinman

manipulator in contact with an x–y table. Experiments were performed in which the robot was programmed to move along the tangent to the table while step increases of force normal to the table were commanded. The system settled at the commanded levels of 1, 5, and 10 N normal force in times ranging from 150 to 330 ms. Force overshoot was evident with errors up to 1.5 N. Tests in which the robot was programmed to maintain a constant force against the table as it was ramped away at a velocity of 1.3 cm s^{-1} resulted in similar force errors. The response times and error levels of the hybrid position/force controlled robot were similar to the performance of the system described in this paper.

Hybrid position/force control requires an explicit description of the workpiece in terms of position and force constraints. This description may be conceptually straightforward; e.g., maintain a constant normal force of 5 N while traveling at a tangential speed of 3 cm s^{-1}. Translating these conceptual descriptions into a form the control system understands is computationally difficult for all but simple tasks. This area is not dealt with in this paper and needs further research.

B. Impedance Control

Impedance control is a general approach to robot motion and force control that attempts to make a manipulator behave as a mass–spring–dashpot system whose parameters (inertia–stiffness–damping) can be specified arbitrarily. A simple example would be to give a robot arm spring-like characteristics. A large spring constant results in a stiff arm; a small constant results in a soft arm. Position and force control are considered two forms of impedance control. Position control implies very high impedances, while force control implies the opposite. The unified approach of impedance control and its implementations are discussed by Hogan [9].

Impedance control has not been implemented in its full form. That is, no one has developed a manipulator in which inertia, stiffness, and damping are simultaneously controlled. Linearized versions consisting of controlled stiffness schemes have been developed by Paul and Shimano [14], Andrews [1], and Salisbury [17]. A controlled damping scheme is described by Whitney [20]. The merits of impedance control strategies are contrasted to those presented in this paper later in this section.

C. Joint Torque Control

This control method alters the torque of individual servo motors to achieve force control at the endpoint of an arm. The torque changes can be calculated using either computed torque methods [13] or direct feedback methods. Luh, Fisher, and Paul [11] and Wu and Paul [22] implemented torque control on two axes of a Stanford manipulator by adding a torque feedback loop to the axis position control loop. Strain gauges placed on the shaft between the motor and the speed-reducing harmonic drive measured the motor torque, which was fed back to the position control loop. The system was not used to control the force applied to the environment but rather to reduce the effect of frictional torques in the robot's motor-tachometer assembly.

The drawback of the torque measurement described above is that the strain gauges were measuring motor, rather than load, torque. Control of tool/workpiece contact forces requires precise knowledge, in the form of accurate models, of arm dynamics, stiffness, and internal friction. While this type of control scheme is adequate for reducing the level of frictional torques, its applicability to manufacturing operations in which force is to be accurately controlled has not been proven.

D. Position/Force Control via Sensor Programming

This approach involves the programming, storage, and execution of force information in addition to motion commands. Hirzinger and others [8], [15], [19] have developed a pair of force sensors: one mounted to a fixed surface, manipulated by a human operator; another, mounted to the wrist of a robot, measured the forces between the robot and workpiece. The differences between the sensor measurements were used to derive robot motion commands.

Such a strategy has been implemented on a five-axis robot and used for deburring of iron castings. The benefits of position/force programming compared to position-only programming methods are reported to be adaptation for grinding wheel wear and time savings in the overall grinding operation.

E. Comparisons with Present Research

The similarities and differences between the above research and the present work can be illustrated with an example: a robot is to follow the surface of a workpiece with a prescribed tangential speed and normal force. In hybrid position/force control it is necessary to define position and force constraints with respect to the surface. The system will then actuate the robot axes to maintain the desired speed and force. The system developed in this work is also a hybrid controller. The specification of force and position constraints are not an explicit part of the control system architecture. Instead, tasks are programmed at certain speeds, and force normal to a surface is maintained. Like hybrid control, this system performs well with simple geometries, but needs more advanced strategies to handle complex workpieces.

In controlled stiffness systems the normal force is proportional to the difference between surface and reference positions. The constant of proportionality is the desired stiffness of the robot. Constant stiffness controllers are not integrating controllers: if the workpiece orientation is altered the desired normal force is not maintained. The controller described herein is integrating and can maintain a constant normal force while tolerating position misalignments.

The similarity between the joint torque control technique and this work is the manner in which the position control is implemented on an individual axis level. Both involve adding an additional feedback loop that interjects position changes into the primary position loop. One fundamental difference is the point of force measurement. Joint torque control uses motor torque measurements which are only equal to load torques if transmission elements are dynamically rigid. This is not the case for most robots.

Systems programmed with a pair of force sensors are able to

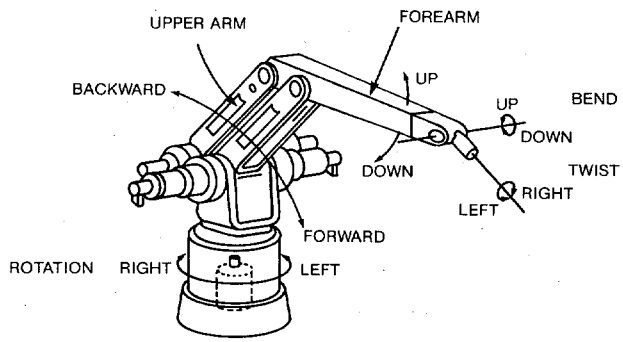

Fig. 3. Five axes of the force controlled robot.

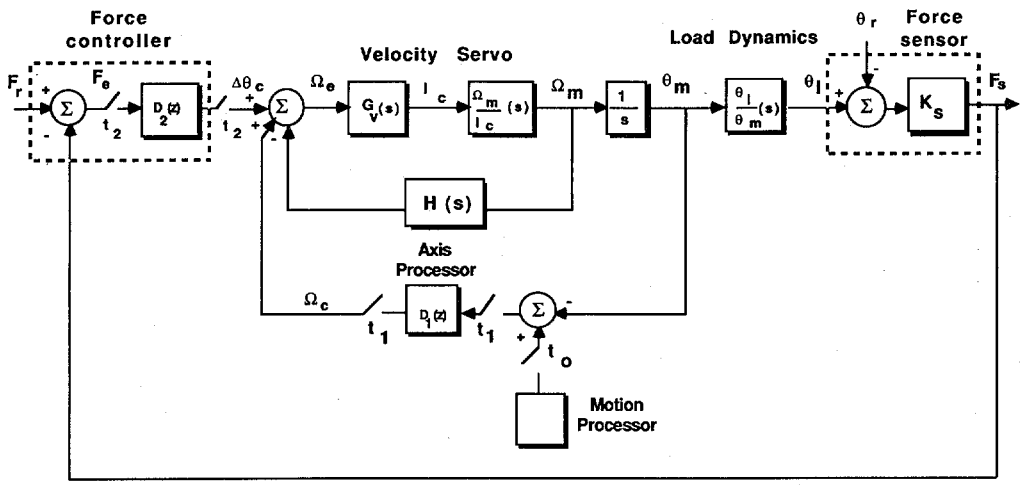

Fig. 4. Block diagram of force control loop interfaced to position control loop.

follow a surface with a desired normal force. Since such systems store position as well as force information, they should be able to follow more complex geometries than the system in this work. The success of these systems is unknown.

III. Single Axis Force Control

As a starting point for developing a multi-degree-of-freedom force controlled manipulator, force control was implemented on single axes of the robot. The five robot axes, shown in Fig. 3, may be classified into two types: resonant and nonresonant. Resonant axes (rotation, upper arm, and forearm) exhibit significant dynamic coupling between motor and load through compliant harmonic drives. Nonresonant axes (twist and bend) do not exhibit such coupling [6]. In the following section force control laws are developed for each type of axis.

A. Nonresonant Axis Force Controller Design

The control problem for the nonresonant axis is posed in the context of Fig. 4. This figure contains the position control loop of Fig. 2 redrawn for force control: blocks for a force controller and force sensor were added; the axis and motion processor blocks were moved to the feedback path. The requirement of the force controller is to calculate discrete position changes $\Delta\Theta_c$ to keep a prescribed reference force F_r between the robot's end effector Θ_l and the reference (workpiece) position Θ_r. The force sensor provided force inputs F_s to the controller by measuring the difference between Θ_r and Θ_l through its mechanical stiffness K_s.

The block diagram includes blocks in both the continuous and discrete time domains. Since the force control loop was implemented in a digital microprocessor, the discrete time equivalents of continuous time transfer functions were obtained by standard numerical or analytical procedures. In the control design the sampling time of the force controller t_2 was set equal to the delay of the axis processor block (10 ms). Hence, the axis processor block was represented as a pure time delay z^{-1}. Note that the motion processor interjected disturbances into the force control loop but did not affect its dynamics.

The dynamics of the velocity servo, load dynamics, and tachometer feedback modules were developed by measuring amplifier gains and transfer functions within the robot position controller. These measurements were obtained by standard identification techniques. Analytical expressions were then fitted to the measurements. For more details see [6] and [18].

Nonlinear dynamic models of the five-axis robot have been previously developed in [6] and [7]. Examples of nonlinearities include tachometer dead zones, torque limits on servo motors, and frictional damping on rotational inertias. For the purposes of model development and compensator design, linearized models were assumed. The effect of the nonlinearities was assessed through simulation and is discussed in Section IV.

For the nonresonant twist axis the load position Θ_l was directly proportional to motor position Θ_m. Thus the transfer function between the two was a constant representing the gear ratio n of the drive:

$$\frac{\Theta_l(s)}{\Theta_m(s)} = \frac{1}{n}. \tag{1}$$

Note that these load dynamics were not the same for the resonant axes discussed below.

The measured frequency characteristics of the twist axis can be represented by an amplitude-dependent first-order transfer function between the motor velocity Ω_m and the current command I_c. For the small amplitude motions typical of force control applications:

$$\frac{\Omega_m(s)}{I_c(s)} = \frac{3.44}{\left(\frac{s}{75.4}+1\right)}. \tag{2}$$

Note that all the transfer functions in this paper are represented as combinations of first- and second-order transfer functions using the following notation:

$$K(a)[\zeta, \omega_0] = K\left(\frac{s}{a}+1\right)\left[\left(\frac{s}{\omega_0}\right)^2 + 2\zeta\left(\frac{s}{\omega_0}\right)+1\right],$$

where K is a constant, (a) is the corner frequency of a first-order transfer function, and $[\zeta, \omega_0]$ are the damping ratio and natural frequency of a second-order transfer function. Using this notation, (2) becomes:

$$\frac{\Omega_m(s)}{I_c(s)} = \frac{3.44}{(75.4)}. \tag{2}$$

Such model transfer functions compare favorably with the measured frequency characteristics as shown in [6].

Closing the velocity loop yielded the transfer function from velocity command Ω_c to the motor position Θ_m of the twist axis as

$$\frac{\Theta_m(s)}{\Omega_c(s)} = \frac{12.5\ (89)\ (113)}{(0)\ (33.4)\ [0.95,\ 102]}. \tag{3}$$

The environment was assumed to be infinitely stiff compared to the compliance of the robot's drive system and the force sensor.

The design of a discrete force compensator $D_2(z)$ was based on root locus design techniques. Figure 5(a) is a z-plane root locus of the twist axis position control loop under proportional control. The locus shows that the system was unstable at a closed loop gain of 14. For lower gains the system was marginally stable, with the locus close to the unit circle. The design goal was to bring the locus into a region of greater stability. Consideration was given to 1) response time, which for a tracking system should be faster than the frequency of the position inputs and 2) overshoot, which for a force control system should be minimal—ideally zero. In choosing between response time and overshoot, response time dominated since the latter was subject to frictional damping not included in the linear model used for compensator design. This assumption was tested in a simulation of the experiment in which damping effects were included.

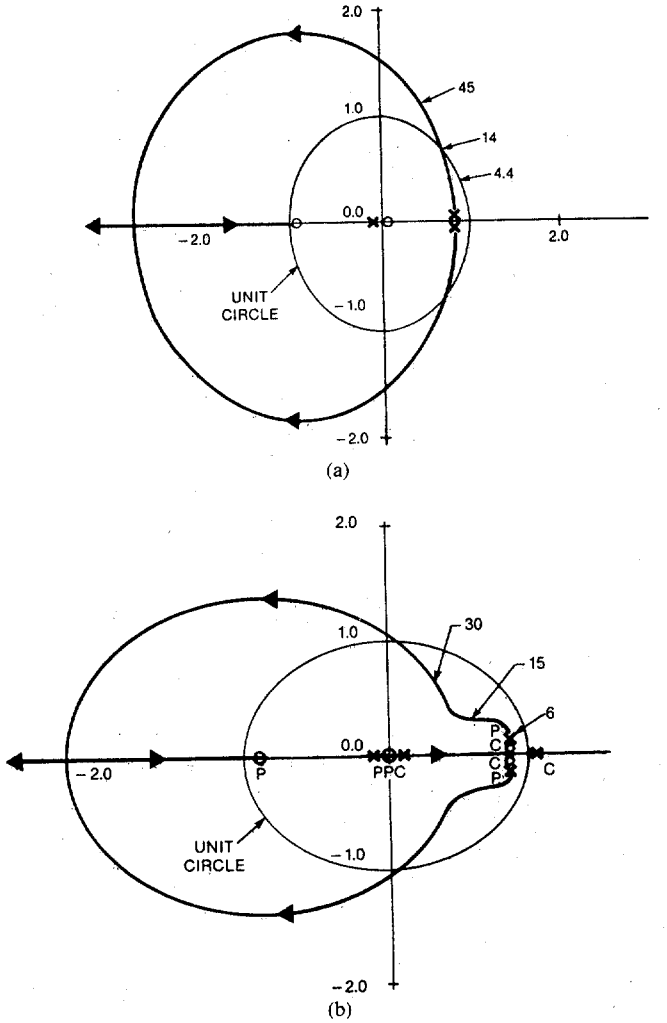

Fig. 5. (a) P control and (b) PID compensated nonresonant axis root loci (P = plant, C = compensator).

Different forms of compensators were investigated and it was decided to choose conventional PID since its implementation was straightforward and it worked well in simulations. A discrete form of a PID compensator for the force control loop is [2]:

$$D_2(z) = \left[K_p + \frac{K_i T}{z-1} + \frac{K_d(z-1)}{T(z-\gamma)}\right] \tag{4}$$

where

K_p	proportional gain
$K_i T$	integral gain
K_d/T	derivative gain
T	sampling period
γ	derivative filter.

This form of PID compensation allows a designer to place two poles and two zeroes. Placing poles at $z = 0$ and 1 included the real axis from $z = 0$ to 1 in the locus. The free integrator $z = 1$ insured zero steady state force error for a

constant desired force. Compensator zeroes needed to be located close to the complex conjugate plant poles in order to draw the locus inward. Pole-zero cancellation was ruled out since the location of the plant poles varied with arm configuration. Various zero locations were tested and the best result was obtained by placing a double zero at $z = 0.82$. The chosen compensator was then:

$$D_2(z) = \frac{(z-0.82)^2}{z(z-1)} . \tag{5}$$

Note that the time constant of the derivative filter did not affect control performance because noise from the force sensor was predominantly comprised of frequencies greater than the bandwidth of control, 10 Hz in this case.

PID compensation produced the root locus of Fig. 5b. Choosing an operating point on the locus required a choice between speed of response and overshoot as mentioned above. At a closed loop gain of six, the response exhibited a damping ratio of 0.6 and a settling time greater than 200 ms. At a gain of 15, the response was less damped and faster, having a damping ratio of 0.4 and a settling time of 150 ms. As noted previously, the overshoot should be reduced by frictional damping, making the root locus at a gain of 15 the region of operation. The closed loop system has positive gain and phase margins of 3.5 dB and 15°, respectively.

B. Resonant Axis Force Controller Design

The rotation axis drive train was similar to the twist axis in that a harmonic drive was the gear reduction mechanism. One difference between the two axes was the relationship between the load and motor inertias. In the rotation axis the rotational inertia of the mass on one side of the harmonic drive was of similar magnitude when referred to the inertia of the motor on the other side. In the twist axis the effective load inertia was much smaller than the motor inertia. Equal inertias on either side of the flexible harmonic drive produced a severe anti-resonance/resonance phenomenon, limiting the dynamic bandwidth of the rotation axis [6].

A dynamic model for the rotation axis has been previously developed [6] based on the four degrees-of-freedom model shown in Fig. 6. In this model the subscripts m and b refer to the elements of the motor and base (rotation) axes, respectively. A torsional spring between the motor and base inertias represents the flexibility of the harmonic drive. The lateral and rotational flexibility between the base and forearm is represented by a second spring with lateral and torsional stiffness and damping. For the force control frequencies of interest in this work (less than 10 Hz) the dominant structural dynamic modes were 1) a rigid body mode in which the motor and base inertias rotate in phase and 2) a torsional mode in which the inertias rotate against each other. A transfer function representing these modes relates motor position Θ_m on one side of the harmonic drive to load position Θ_l on the other side, and can be expressed as:

$$\frac{\Theta_l(s)}{\Theta_m(s)} = \frac{(222)}{n[0.10, 44.7]} \tag{6}$$

where n = gear ratio of the harmonic drive.

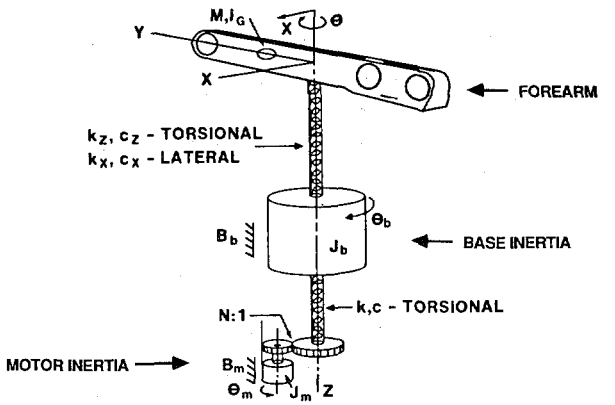

Fig. 6. Four-degree-of-freedom dynamic model for robot arm drive flexibility.

As in the twist axis this transfer function was obtained by independent measurements between specific points of the position control loop. Additional transfer functions were obtained through similar experimental measurements.

A representative transfer function relating the motor velocity Ω_m to motor current I_c for this model is

$$\frac{\Omega_m(s)}{I_c(s)} = \frac{26.7\ [0.10, 44.7]}{(20.7)\ [0.29, 60.1]} . \tag{7}$$

With the velocity loop closed the transfer function from commanded velocity Ω_c to motor position Θ_m is

$$\frac{\Theta_m(s)}{\Omega_c(s)} = \frac{12.5\ (89)\ (113)\ [0.10, 44.7]}{(0)\ (61.2)\ [0.17, 40.3]\ [0.81, 110]} . \tag{8}$$

Note that although the dynamics of the rotation and twist axes are different, the servo position controllers were tuned (by the designers) to give the same motion control bandwidth of 4–5 Hz [6]. This tuning permitted the axes to respond with similar response speed and accuracy in spite of their distinct dynamics.

The root locus of the rotation axis position control loop under proportional control is shown in Fig. 7a. Comparing this figure to the twist axis root locus (Fig. 5(a)), the effect of the different dynamics is clear. The twist axis was stable at gains less than 14. Here the system was unstable at gains greater than 0.9.

The demand on the force compensator was the same as for the twist axis: bring the locus into a region of greater stability. PID compensator poles were once again placed at $z = 0$ and 1. The free integrator assured zero steady state force error. The remaining question was where to place the compensator zeroes. By locating them on the real axis the portion of the locus beginning at $z = 0.75 \pm 0.15j$ and encircling the origin was changed to two smaller encirclements as shown in Fig. 7(b). Both zeroes in this figure were located at $z = 0.7$. This compensator did not change the overall shape of the unstable branches but doubled the magnitude of the gain at which instability occurred. The rotation axis compensator was

$$D_2(z) = \frac{(z-0.7)^2}{z(z-1)} . \tag{9}$$

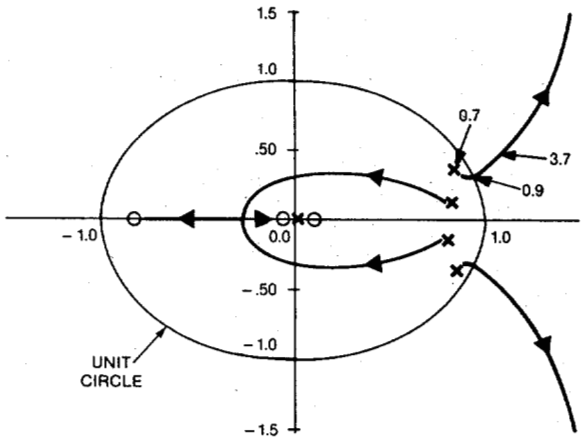

(a)

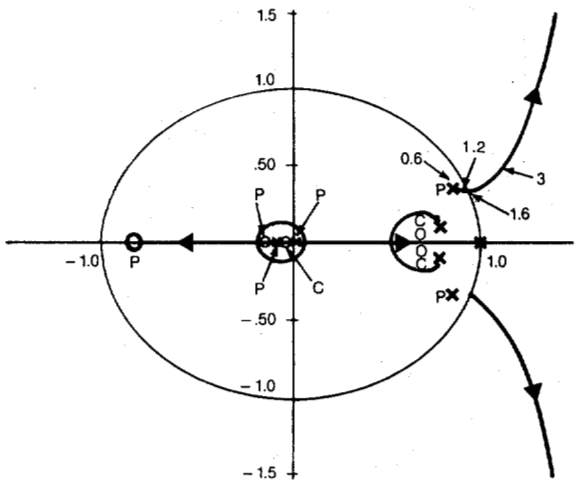

(b)

Fig. 7. (a) P control and (b) PID compensated resonant axis root loci (P = plant, C = compensator)

The system exhibited gain and phase margins close to zero, indicating that the system was marginally stable. Comparing these margins to those of the twist axis, 3.5 dB and 15°, respectively, it was expected that the range of acceptable performance of force control on the rotation axis would be less than that of the twist axis. Subsequent simulations of the force control loop, including drive system friction, showed that the stability margin predicted by the linear analysis was conservative and that acceptable performance could be realized in practice.

IV. Multiple-Degree-of-Freedom Force Control

The initial issue explored in the design of a multiple-degree-of-freedom force controller was the structure within which to implement control. In the previous section force controllers were developed for two types of axes. Single-axis controllers were advantageous because of their simplicity. The drawback of combining single-axis controllers was that dynamic interactions between the axes could not be attributed. In other words, dynamic cross-coupling effects, if they existed, might have propagated disturbances through the system and destroyed control performance. In the single-axis force control experiments dynamic cross-coupling effects were not apparent. For example, force control of the twist axis did not introduce disturbances into the bend axis. To substantiate and quantify this observation further, cross-coupling effects were analyzed. The performance of the system under force control was compared to performance without force control under a complete five-degree-of-freedom nonlinear simulation, using the Simnon program [5]. This analysis is described in the next section. The conclusions of the analysis are validated by the performance of the implemented system.

A. Analysis of Dynamic Cross-Coupling Effects

Modules from the single axis simulations in the previous section were refined and integrated with an existing nonlinear simulation of the robot system [10]. This simulation is shown schematically in Fig. 8. Notice the similarity of the simulation structure with the force control block diagram of Fig. 4. The principal modules are:

Motion processor: Algorithms for performing path generation, interpolation, and inverse coordinate transformation.

Velocity servo: Models of individual axis power electronics and servo controller.

Actuator dynamics: Nonlinear models of electromechanical drive system components including servo motors and transmission elements.

Arm dynamics: Newton–Euler model of the five degree-of-freedom arm and forward coordinate transformation algorithm.

Force control: Force control algorithm including representation of processor arithmetic, truncation, and scaling.

Process: Models of tool/workpiece interaction and force sensor operation.

Analysis of cross-coupling effects was performed by simulating a task in which force control was implemented on a single, isolated axis. The robot's joint angles were observed and compared to simulations of the identical task in which force control was not activated. Only the force controlled axis angles should have deviated from their nonforce control counterparts. Figs. 9(a)–(c) show the rotation, upper arm, and forearm axis angles, respectively, from one simulation. Here, the taught path was parallel to the base of the robot. It was desired to maintain a constant force of 10 N normal to the path. The system maintained the prescribed force by actively servoing the forearm axis. This changed the forearm angles in the force control case compared to the nonforce control case. The rotation trajectory was the same in both cases. The upper arm angle was initially affected by active control of the forearm axis. This effect faded after the initial transient. The bend and twist angles, whose respective trajectories were exactly the same, are not shown.

Similar tasks, with different axes and combinations of axes under force control, were simulated in other portions of the robot's working envelope. The speed and force ranges in the simulations were 1 to 9 cm s^{-1} and 1 to 15 N. Simulation results indicated no significant dynamic cross-coupling characteristics between the axes of the robot. There was mild

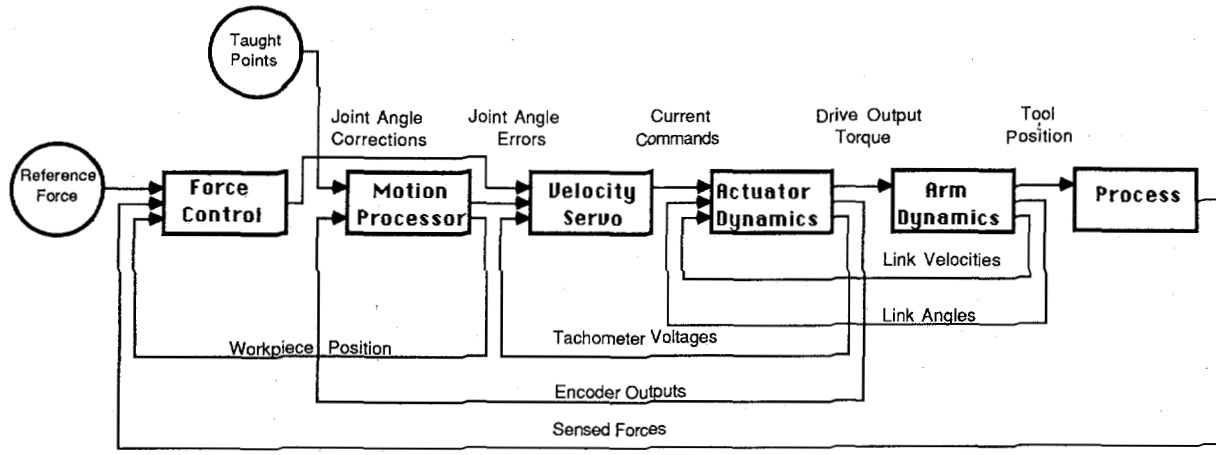

Fig. 8. Dynamic simulation of force control system.

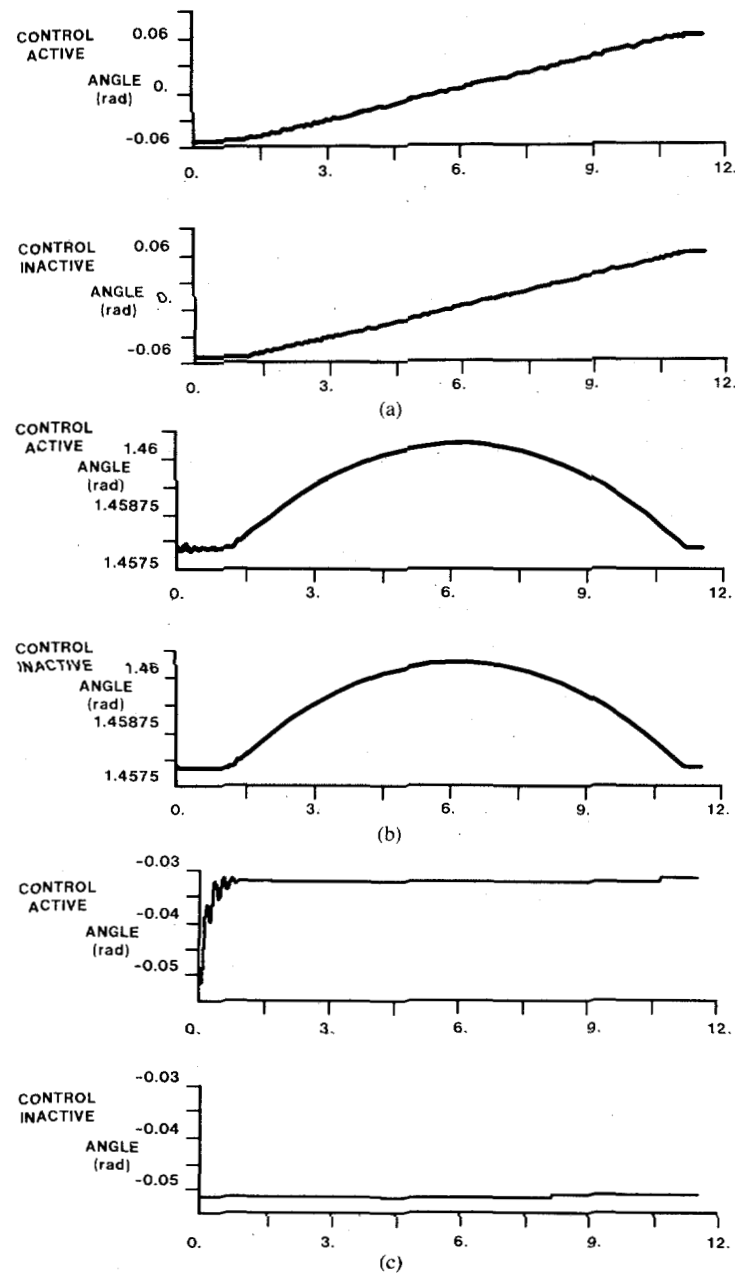

Fig. 9. Simulations of robot angles with and without force control activated. (a) Rotation axis. (b) Upper-arm axis. (c) Forearm axis.

coupling between the upper arm and forearm axis as indicated above. This effect was strongest when the upper arm was under force control and the forearm was not. This is a reasonable result since a move of the upper arm necessitated an opposite move of the forearm, whereas the forearm could be moved without moving the upper arm.

After confirming that cross-coupling effects were minimal, design of a multiple-axis compensator as a series of single loop compensators began. The dynamic behavior of the bend axis was similar to that of the twist axis: a first order lag with a gradual roll off in magnitude and phase at frequencies greater that 7–8 Hz. The dynamic characteristics of the upper arm and forearm axes were similar to the rotation axis since the rotational inertias on either side of the harmonic drive were equivalent, producing a strong antiresonance/resonance feature in the frequency response. Equivalent dynamic behavior between the axes allowed the control designs of the previous section to be used. The control gains were tuned to accommodate the relative differences of harmonic drive gear ratios, rotational inertias, and other physical quantities.

C. Coordinate Transformations

Three coordinate systems were used to transform the orientation of the forces at the deburring tool/workpiece interface to forces in the robot's joint coordinate system. Frame XYZ_g is the global coordinate frame of the robot. The frame's origin is located at the base of the robot. Frame XYZ_s is the force sensor coordinate frame, whose origin is located at the base of the sensor mounted on the end of the robot's wrist. Frame XYZ_t is the tool coordinate frame, the origin of which is located at the tip of the deburring bit. The relationship between these frames was as follows: the force sensor measured forces in XYZ_s caused by deburring tool-workpiece interactions in XYZ_t. It was desired to control those interactions in the frame of the workpiece referenced in the global coordinate frame XYZ_g. Thus it was sought to control force in XYZ_g given force measurements in XYZ_s.

The transformations between the three coordinate frames were derived by standard mathematical techniques. The results of the transformations were sensed forces in robot joint coordinates which were directed as inputs to the individual force control loops.

V. Experimental Results

A. Edge Following Experiments

The initial series of experiments tested the ability of the system to maintain a specified normal force while following the edge of a workpiece. These tests served as a baseline for subsequent deburring experiments. The force error, the difference between desired and actual normal force, was the target variable in these tests. The experiments were performed over a range of tangential speeds, 1 to 9 cm s^{-1}, and normal forces, 1–15 N, that were realistic for deburring.

Figure 10 contains two oscilloscope traces of a typical edge following experiment. The upper trace is the ac component of rms force error. The lower plot is the normal force history during the pass. The particular speed and force level for this figure were 6 cm s^{-1} and 15 N, respectively. The edge to be

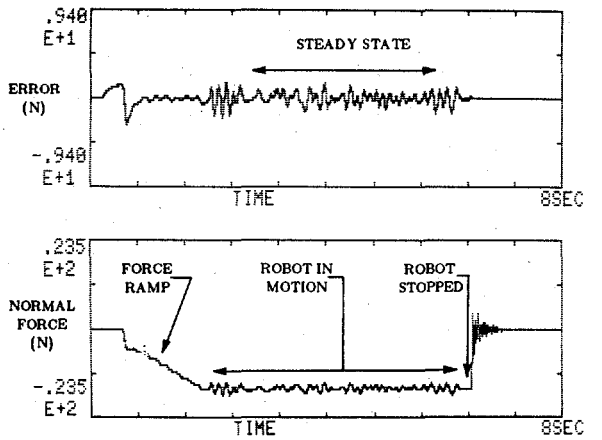

Fig. 10. Experimental measurements of force errors and contact force during an edge following experiment.

followed was a metal bar located in the global XY frame. The robot was brought close to the workpiece, force control was initiated, and the commanded force was ramped from zero to the programmed level. During this ramp the robot was stationary. Once the normal force reached the set point, the robot moved along the workpiece. Notice that the force error increased as the robot accelerated. At the end of the pass, the robot stopped and force control was deactivated. The rms value of the force error was measured only during steady state operation, when the robot was moving at the desired speed and the normal force reached its set point. This measurement thus excluded the effects of the force transients.

Figure 11 is a plot of the rms force error vs. travel speed at increasing levels of normal force. The salient feature of this figure is the increase of force error with increasing travel speed. At these speeds the system was able to maintain the desired force within the error shown. Increasing travel speed introduced disturbances with higher frequency content. As disturbances were encountered above the cutoff frequency of the force controller, the rms force errors increased. Notice that the force errors did not increase with increasing normal force. This result indicates that the force control system behaved in a linear manner, responding similarly over a range of reference forces.

The performance of this system was similar to that of the hybrid position/force control system described in [4] and [16]. The force errors incurred in following a surface fall into the same range, 0–2 N. In addition, both systems show the ability to control force over a wide range: 0–10 N for hybrid control, 0–15 N in this work.

B. Deburring Experiments

The edge following experiments described the performance of the force control system in maintaining programmed forces at increasing tangential speeds. The deburring experiments tested this ability with the added dynamic interaction between the tool and workpiece. These experiments were designed similar to deburring operations performed in industry. A bar of a high-strength superalloy used in high temperature aircraft engine components was the metal to be deburred. A conical shaped carbide cutting tool was used to deburr the edge of a 27

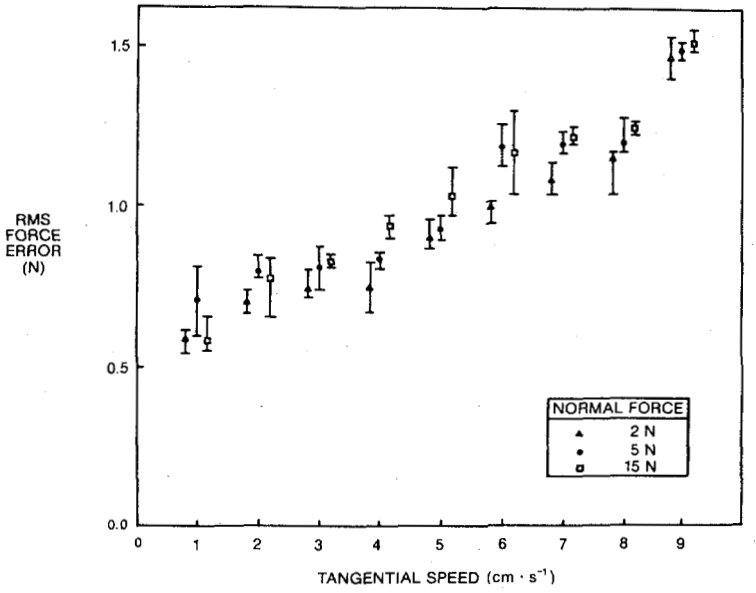

Fig. 11. rms force error vs. tangential speed during an edge following experiment.

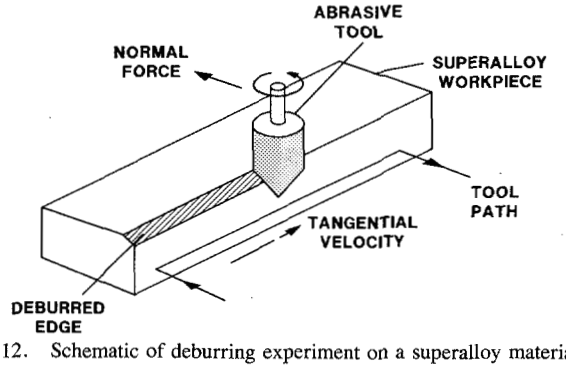

Fig. 12. Schematic of deburring experiment on a superalloy material.

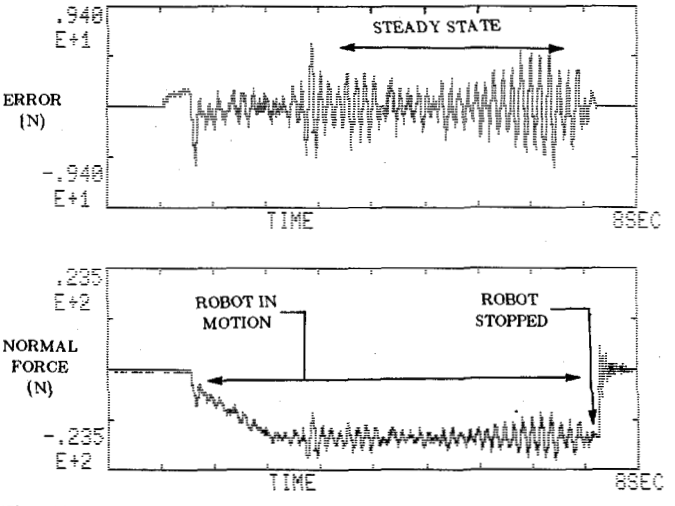

Fig. 13. Experimental measurements of force errors and contact force during a deburring experiment.

cm section of the sample. The bar was located in the global XY frame of the robot. Figure 12 is an illustration of the experimental setup. The robot path was similar to that used in the edge following experiments in that the robot moved toward the workpiece, force control was initiated by ramping the force to the desired level, and the deburring pass was performed. Note that the robot did not stop as the force was ramped from zero to the set point as in the edge following case. Experiments were performed at two force levels, 5 and 15 N, across a range in speed from 1 to 9 cm s^{-1}. The normal force was limited to 15 N because at higher levels the force was sufficient to stall the tool bit. Note that the deburring process and not the control system performance was the limitation toward achieving higher speeds and greater normal forces. Force errors and force histories during a typical deburring pass are shown in Fig. 13. The particular speed and force level for this figure were 6 cm s^{-1} and 15 N, respectively.

The principal difference between deburring and edge following passes was that deburring increased the amplitude of force errors substantially. This can be seen by comparing Figs. 13 and 10. Force errors encountered during deburring are plotted in Fig. 14. Force errors for the edge following

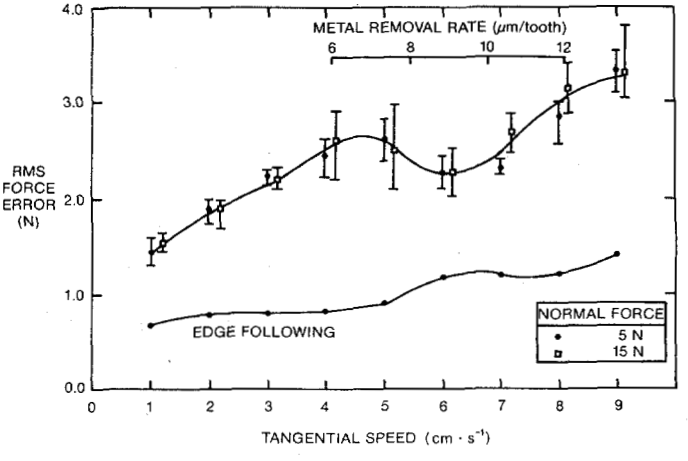

Fig. 14. rms force error vs. tangential speed during deburring experiments.

experiment are included in this figure for comparison. The behavior of the deburring force errors is marked by a gradual increase up to a speed of 4 cm s^{-1}, followed by a decrease between 5 and 7 cm s^{-1}, and an increase for speeds greater than 8 cm s^{-1}. The valley centered near 6 cm s^{-1} indicates that certain speeds were more desirable than others from a force error point of view (the deburring process was smoother).

It is interesting to compare the range of reduced force errors with recommended feed rates for the particular tool and metal used in the experiment [3]. Surface deburring speeds for hard steels should be in the range of 20-30 m min^{-1} (70-100 ft min^{-1}). Given the geometry of the carbide tool (diameter = 8.3 mm) and the rotational speed of the deburring tool in contact with the metal (17 000 rpm), a feed rate of 6 cm s^{-1} translates into a metal removal rate of 9 μm per tool tooth. Suggested metal removal rates for deburring operations fall between 6 and 12 μm (0.00025 to 0.0005 in) per tooth. A metal removal rate scale is superimposed onto Fig. 14. This comparison indicates that the decrease in force errors occurs in the same range of specified feed rates for typical deburring operations. Correlating this decrease in force error with the quality of the deburring process (surface finish) is a logical step requiring further study.

Deburring tools other than carbide bits were also investigated. Figure 15 is a photograph of an emery wheel deburring a piece of steel. An emery wheel is typically used for the light removal of metal, for example in polishing operations. The force errors encountered during deburring with an emery wheel were of the same magnitude as errors found using a carbide tool.

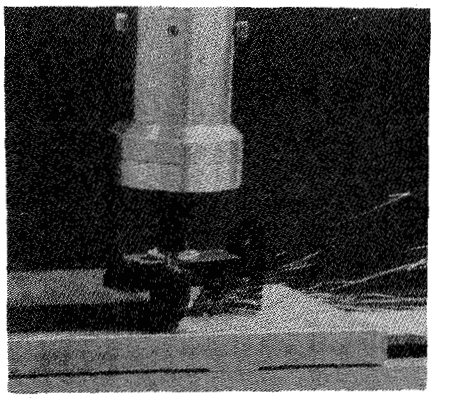

Fig. 15. Photograph of deburring operation with an emery wheel.

VI. Conclusion

The major results presented in this paper are as follows.

- A microprocessor-based force control system was developed to operate in parallel with the position control system for the individual axes of a robot. Interfacing the external position commands to the position control loop was accomplished so that other system features such as motion bandwidth, programming, and safety remained undisturbed.
- A stable force compensator was designed under specific constraints including dynamic limitations imposed by drive train flexibility and a fixed architecture of the existing robot controller. Additional hardware necessary to achieve closed-loop force control was modest.
- Multiple-degree-of-freedom force control was designed using single axis loops after it was verified that dynamic cross-coupling between the robot axes was minimal. The single loop approach to multiple-degree-of-freedom force control resulted in a straightforward control algorithm.
- The force control system was tested in edge following experiments. Force errors remained constant across a range of normal force from 1 to 15 N. These force errors increased with increasing tangential speed.
- Deburring experiments indicated a range of deburring speeds within which force errors were reduced. This range falls within the recommended speed range for other types of deburring operations. The deburring process, not the control system, was the limiting factor in achieving increased deburring speeds and higher normal forces.

References

[1] R. J. Andrews, "Douli systems: design and construction of a manipulator and controller for research in impedance control," S.B. thesis, Dept. Mechanical Engineering, Massachusetts Institute of Technology, Cambridge, June 1981.

[2] K. J. Astrom and B. Wittenmark, *Computer Controlled Systems—Theory and Design*. Englewood Cliffs, NJ: Prentice-Hall, 1984.

[3] T. Baumeister, *et al.*, Eds, *Mark's Standard Handbook for Mechanical Engineers*, 8th ed. New York, NY: McGraw-Hill, 1979.

[4] J. J. Craig and M. H. Raibert, "A systematic method of hybrid position/force control of a manipulator," in *Proc. IEEE Computer Software & Appl. Conf.*, pp. 446–451, Nov. 1979.

[5] H. Elmquist, "SIMNON: an interactive simulation program for nonlinear systems," Dept. Automatic Control, Lund Institute of Technology, report 7502, Lund, Sweden, 1975.

[6] M. C. Good and L. M. Sweet, "Structures for sensor-based robot motion control," in *Proc. 1984 Amer. Contr. Conf.*, vol. 1, pp. 23–31, June 1984.

[7] M. C. Good, L. M. Sweet, and K. L. Strobel, "Control system models for integrated robots and drive systems," *ASME J. Dynamic Syst., Measurement, Contr.*, vol. 107, pp. 53–59, Mar. 1985.

[8] G. Hirzinger and J. Heindl, "Sensor programming—a new way for teaching robot paths and forces/torques simultaneously," presented at The Third International Conference on Robot Vision and Sensory Controls, Cambridge, MA, Nov. 1983.

[9] N. Hogan, "Impedance control: an approach to manipulation: Part I—theory, part II—implementation, part III—applications," *ASME J. Dynamic Syst., Measurement, Contr.*, vol. 107, pp. 1–24, Mar. 1985.

[10] I. Imam, *et al.*, "Simulation and display of dynamic path errors for robot motion off-line programming," in *Proc. Robots 8*, vol. 1, pp. 4-28-4-44, June 1984.

[11] J. Y. S. Luh, W. D. Fisher, and R. P. C. Paul, "Joint torque control by a direct feedback for industrial robots," *IEEE Trans. Automat. Contr.*, vol. AC-28, no. 2, pp. 153–161, Feb. 1983.

[12] M. T. Mason, "Compliance and force control for computer controlled manipulators, *IEEE Trans. Syst., Man, Cybern.*, vol. SMC-II, No. 6, pp. 418–432, June 1981.

[13] R. P. C. Paul, "Modeling, trajectory, calculation, and servoing of a computer controlled arm," Artificial Intelligence Laboratory, Stanford University, Stanford, CA, memo 177, Sept. 1972.

[14] R. Paul and B. Shimano, "Compliance and control," in *Proc. 1976 Joint Automatic Contr. Conf.*, pp. 694–699, 1976.

[15] G. Plank and G. Hirzinger, "Controlling a robot's motion speed by a force-torque-sensor for deburring problems," in *Proc. 4th IFAC/IFIP Symp. Informat. Contr. Problems in Manufacturing Tech.*, pp. 97–102, Oct. 1982.

[16] M. H. Raibert and J. J. Craig, "Hybrid position/force control of manipulators," *IEEE Trans. Syst., Man, Cybern.*, vol. SMC-II, no. 6, pp. 418–432, June 1981.

[17] J. K. Salisbury, "Active stiffness control of a manipulator in Cartesian

coordinates," in *Proc. 19th IEEE Conf. Decision Contr.*, vol. 1, pp. 95–100, Dec. 1980.
[18] T. M. Stepien, "A microprocessor-based control system for robotic deburring," S.M. thesis, Department of Mechanical Engineering, Massachusetts Institute of Technology, Cambridge, Sept. 1984.
[19] C. Thiessen, "Improving grinding performance of an ASEA-robot by two-dimensional sensor controlled path correction," in *Proc. 3rd IFAC/IFIP Symp. Contr. Problems Devices Manufacturing Tech.*, pp. 265–270, 1980.
[20] D. E. Whitney, "Force feedback control of manipulator fine motions," *ASME J. Dynamic Syst., Measurement, Contr.*, vol. 99, pp. 91–97, June 1977.
[21] ——, "Historical perspective and state of the art in robot force control," in *Proc. IEEE Int. Conf. Robotics Automat.*, pp. 262–268, Mar. 1985.
[22] C. H. Wu and R. P. Paul, "Manipulator compliance based on joint torque control," in *Proc. 20th IEEE Conf. Decision Contr.*, vol. 1, pp. 265–270, Dec. 1981.

Thomas M. Stepien (S'84–M'84) received the S.B. and S.M. degrees in mechanical engineering from the Massachusetts Institute of Technology, Cambridge, in 1983 and 1984, respectively.

He was with the Control Theory and Systems Program at the General Electric Corporate Research & Development Center as a part of M.I.T.'s Engineering Internship Program. He is currently a staff member in the Robotics and Assembly Systems Division of The Charles Stark Draper Laboratory, Inc., Cambridge, MA. His principal activities include applied research on advanced assembly equipment, automated robotic deburring and grinding, expert systems, and consulting on industrial automation issues.

Mr. Stepien is a member of the American Society of Mechanical Engineers and Robotics International/Society of Manufacturing Engineers.

Larry M. Sweet (M'83) received the B.S. degree in mechanical engineering from the University of California at Berkeley in 1969 and the S.M. and Ph.D. from the Massachusetts Institute of Technology, Cambridge, in 1971 and 1974, respectively.

He is Manager of Knowledge-Based Systems Branch at the General Electric Corporate Research and Development Center, Schenectady, NY. Previously he was Manager of GE's Control Theory and Systems Program, where he directed work on sensor-based controls for robots and automated manufacturing systems. Prior to that he was an Associate Professor in the Department of Mechanical and Aerospace Engineering at Princeton University.

Dr. Sweet was elected a Guggenheim Foundation Fellow in 1981, has authored numerous technical papers and has received many awards, notably an IR 100 award in 1984 as co-developer of the General Electric TIC Welding Vision System.

Malcolm C. Good received the B.S., M.S., and Ph.D. degrees in mechanical engineering from the University of Melbourne, Melbourne, Australia.

He is currently a Principal Research Scientist with the Division of Manufacturing Technology of the Australian Commonwealth Scientific and Industrial Research Organization, Melbourne, Australia. He was previously a professor in The Department of Mechanical and Industrial Engineering of The University of Melbourne.

Dr. Good's research interests include vehicle dynamics, human factors of automobile and motorcycle control, vehicular impacts with roadside structures, and the dynamics and control of industrial robots. The research reported in this paper was performed while he was a Visiting Research Fellow at the Control Theory and Systems Program of General Electric Corporate Research and Development Center.

Masayoshi Tomizuka (M'86) received the B.S. and M.S. degrees in mechanical engineering from Keio University, Tokyo, Japan in 1968 and 1970, respectively. He received the Ph.D. degree in mechanical engineering from the Massachusetts Institute of Technology, Cambridge, in 1974.

He is currently a Professor in the Department of Mechanical Engineering at the University of California, Berkeley, CA. His research interests include digital and adaptive control with application to mechanical systems including robotic manipulators and machine tools.

Dr. Tomizuka currently serves as Chairman of the Executive Committee of the Dynamic Systems and Control Division of the American Society of Mechanical Engineers and is an Associate Editor of the *IEEE Control Systems Magazine.* He has authored over 50 technical papers and co-authored *Theory and Practice of Adaptive Control* (in Japanese) with I. D. Landau.